Enabling Proprioception in Multistable Soft Machines Through Embedded Soft Capacitive Sensors

Hugo de Souza Oliveira[®], *Member, IEEE*, Xin Li, *Graduate Student Member, IEEE*, Niloofar Saeedzadeh Khaanghah, Niko Münzenrieder[®], *Senior Member, IEEE*, and Edoardo Milana[®], *Member, IEEE*

Abstract—Transforming soft machines into fully autonomous soft robots capable of complex interactions with the environment requires the integration of soft electronics and sensors, enabling feedback control while preserving mechanical compliance. Multistable mechanisms, such as mechanical metamaterials and snapping beams, are great candidates for such systems due to their programmable nonlinear responses. In this work, we introduce the integration of a sensing technology based on 3D-printed soft capacitive sensor in a 3-D-printed multistable metastructure composed of four bistable unit cells-enabling proprioceptive monitoring of state transitions by detecting snapthrough events in multistable mechanisms. Under cyclic tensile loading, the metastructure exhibits snapping events at forces up to 7 N, accompanied by capacitance changes from about 0.025 to 0.750 pF. We further demonstrate the integration of the same sensing principle in a 3-D-printed monolithic bistable soft gripper, reliably grasping delicate objects such as popcorns, tomatoes, and strawberries, spanning masses from 0.5 to 16 g. These results confirm that embedded capacitive soft sensors are a viable technology to detect snap-through transitions and to be seamlessly integrated in soft structures, representing a crucial step toward fully compliant, self-aware robotic systems.

Index Terms—Bistable grippers, mechanical metamaterials, soft capacitors, soft robotics.

I. INTRODUCTION

OFT robotics is a promising technology in fields that require delicate, adaptive, and safe interaction with the environment [1]. Using compliant materials instead of rigid components, soft robots are uniquely suited for applications in the food industry [2], minimally invasive surgery [3], ocean exploration [4], among others. Unlike conventional robots that rely on torque or impedance control to ensure safe contact, soft robots inherently embrace mechanical compliance [5]. Given their monolithic structure, design principles of soft robotics

Received 17 June 2025; accepted 10 July 2025. Date of publication 17 July 2025; date of current version 7 October 2025. This work was funded by the Deutsche Forschungsgemeinschaft (DFG, German Research Foundation) under Germany's Excellence Strategy—EXC-2193/1–390951807. (Corresponding author: Edoardo Milana.)

Hugo de Souza Oliveira, Xin Li, and Edoardo Milana are with the Cluster of Excellence livMatS@FIT, Freiburg Center for Interactive Materials and Bioinspired Technologies, University of Freiburg, 79110 Freiburg, Germany, and also with the Department of Microsystems Engineering—IMTEK, University of Freiburg, 79110 Freiburg, Germany (e-mail: milana@imtek.de).

Niloofar Saeedzadeh Khaanghah and Niko Münzenrieder are with the Faculty of Engineering, Free University of Bozen-Bolzano, 39100 Bolzano, Italy.

This article has supplementary downloadable material available at https://doi.org/10.1109/JFLEX.2025.3589993, provided by the authors.

Digital Object Identifier 10.1109/JFLEX.2025.3589993

can be applied to both large-scale (> 1 m) [6] and small-scale (< 1 mm) [7] systems. Advances in soft robotics are driven by progress in engineering devices made from soft materials [8].

Indeed, in recent years, soft robotic systems have begun to leverage the properties of soft materials beyond the mere mechanical compliance, harnessing the intrinsic nonlinearities of soft matter to expand their functionalities in terms of actuation, sensing, and control [9]. Structures such as balloons, slender beams, tubes, and shells exhibit highly nonlinear force—displacement relationships with peaks and valleys, enabling snap-through instabilities that can be exploited to amplify motion [10], [11], generate jumps [12], trigger sequences [13], [14], and produce self-oscillations [15], [16]. However, these behaviors are typically programmed by design and operate in open-loop, without sensing or feedback.

For soft robots to operate autonomously in unstructured environments, feedback mechanisms are essential. As in traditional robotics, sensing plays an important role in coupling with actuation to enable closed-loop control [17], [18]. However, while soft actuators and structures are a well-established technology in soft robotics, the sensors and control elements still rely on traditional electronics, which is stiff and bulky, and use fabrication methods that are not compatible with soft materials. These limitations hinder the full integration of sensors in soft robotics due to mechanical and process incompatibilities. However, such limits are being challenged by the recent advances in soft and flexible electronics [19], [20], [21], which have enabled the development of thin, lightweight, transparent, and even eco-friendly sensors [22], [23]. These sensors hold potential to be seamlessly integrated into compliant robotic bodies. Embedding such electronics allows soft systems to gain proprioception (self-sensing of internal state) and exteroception (perception of the environment), enabling new levels of adaptability. Moreover, advances in additive manufacturing and materials science are enabling new fabrication processes, which allow straightforward production of monolithic functional soft robots [24], [25], [26].

Attempts of integrating soft sensors with multistable soft machines focused on different approaches; dielectric materials [27], [28], liquid metal [29], capacitive plates [30], hydrogels [31], microfluidic transmission [32], soft optoelectronics [33], and strain sensors [34], [35], [36]. Each method has its

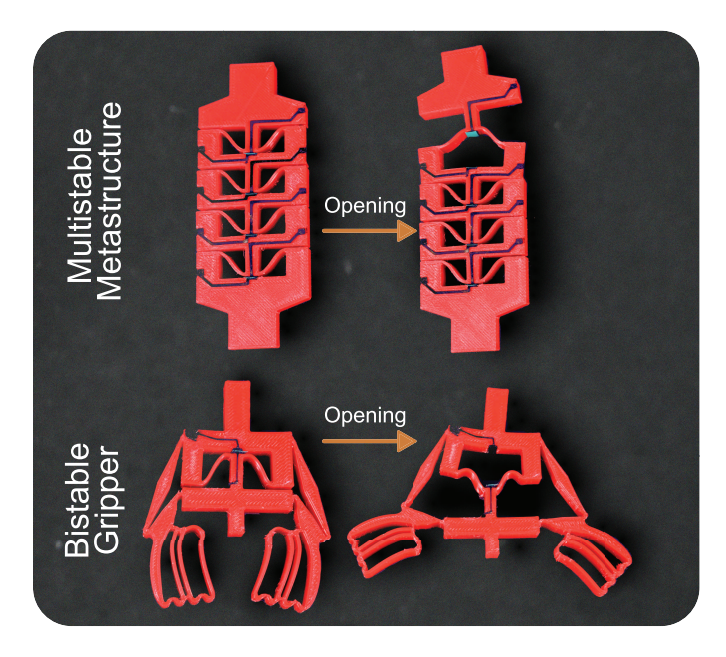


Fig. 1. Multistable soft machines with integrated soft capacitive sensors.

disadvantages, in terms of complex manufacturing methods, high costs of materials, or mechanical mismatches, such as delamination or stiffening.

In this work, we aim at introducing a straightforward approach to providing nonlinear, 3-D-printed multistable soft structures with proprioceptive capabilities, specifically the ability to detect snap-through transitions between different states. In this context, we integrate soft sensors in the same embodiment of the multistable soft structure. As such, we need a technology that is compatible with the 3-D printing process used for the structure (fused deposition modeling, FDM) and does not influence the mechanical properties of the structure. Moreover, we do not need to precisely monitor the continuous deformed state of the structure, but only to detect the discrete changes following the transitions between the mechanical states. Given such requirements, we opt for capacitive sensing, using printable conductive composite material, made of the same matrix as the structures. With this approach, the capacitive plates and the soft structures can be fused together, ensuring integration by avoiding delamination and stiffening issues, typical of classical capacitive sensors [30]. As such, the sensor acts as a contactless switch that needs to detect only the change in mechanical state. We first integrate capacitive sensors in a multistable metastructure composed of four bistable unit cells capable of snapping sequentially under tension or compression. Each unit cell incorporates a flexible, printed capacitive sensor that allows the monitoring of the state transitions throughout the structure. Building on the same sensing strategy, we also present a bistable soft gripper as a demonstrator, integrating a flexible capacitive sensor to track its mechanical state during actuation. The gripper is composed of the snapping tensile structure used as unit cell of the metamaterial and a compliant mechanism that converts the linear displacement of the snapping structure in the closing motion of the gripper fingers. The snapping

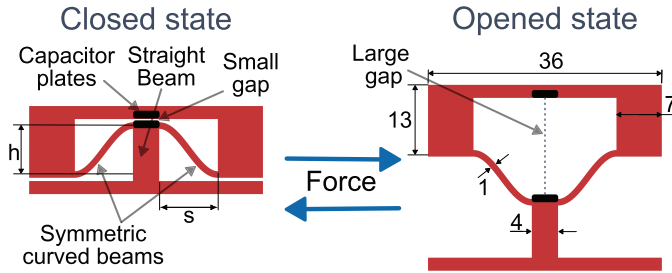


Fig. 2. Bistable unit cell used as building block of the multistable metastructure and the gripper.

structure also behaves as a passive mechanical touch sensor, since the force exerted by the grasped object triggers the closure mechanisms [37], which is in turn detected by the capacitive sensor. Fig. 1 shows the fabricated multistable structure with embedded capacitive sensing, as well as the bistable soft gripper. Moreover, our devices are entirely 3-D-printed using thermoplastic elastomers for both structural and conductive materials, enabling an integrated fabrication process where sensing, actuation, mechanical, and control features can be integrated in the same materials' system.

II. DESIGN AND FABRICATION

The multistable metastructure and the gripper designs integrate as fundamental building block a bistable unit cell [38], [39], [40], consisting of two symmetric curved beams that can snap between two mechanical states when subjected to tensile or compressive loadings, as displayed in Fig. 2. The curved beam *B* is parameterized using the relation

$$B(s) = \frac{h}{2} \left[1 - \cos\left(\frac{2\pi s}{l}\right) \right] \tag{1}$$

corresponding to the shape of the Euler first buckled mode, in which s ranges from 0 to 9 mm, the height h is 8 mm, and the width l is 18 mm. The resulting metastructure has an overall thickness of 7 mm. In addition, the unit cells include integrated grooves designed to accommodate the capacitive sensor plates and their electrical contacts.

The soft capacitor integrated to the structures features two parallel conductive plates separated by a small gap of 0.5 mm in the closed state. As the unit cells transition from closed to open state, the plate separation increases significantly, reaching 15.0 mm, as shown in Fig. 2. The capacitor uses air and a thin vinyl layer as dielectric materials, with the vinyl serving as an electrical insulator between the plates in the closed position. The soft capacitive plates have dimensions of 0.4×7.3 mm and a thickness of 0.4 mm. Both the conductive plates and the corresponding electrical connections are designed to precisely match the geometry of the grooves within the designed structures.

A. Multistable Metastructure

Four unit cells are stacked vertically to enable multistability, as shown in Fig. 3(a). The metastructure, flexible capacitive plates, and electrical connections are 3-D-printed using a Prusa MK4 printer. The structure is fabricated from thermoplastic

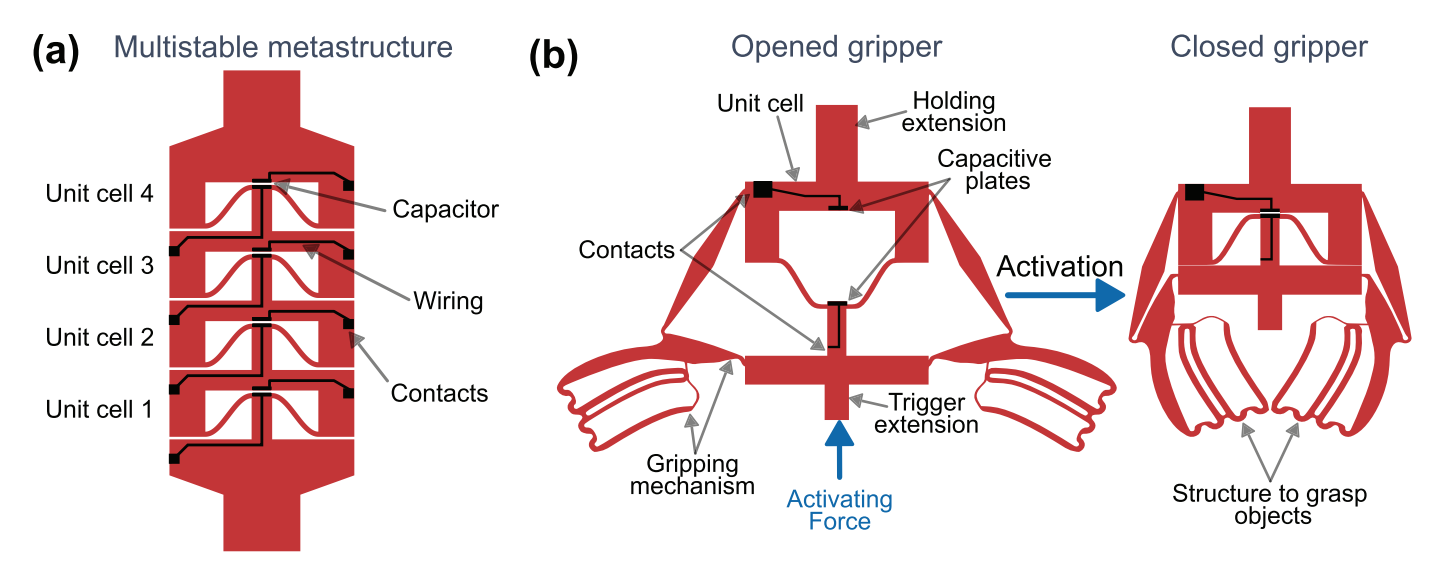


Fig. 3. Design characteristics. (a) Schematic of the multistable metastructure with the capacitors, wiring, and the contacts. (b) Schematic of the gripper in its open and closed configuration to grasp objects.

polyurethane (TPU) filament (NinjaTek Cheetah, Shore 95A) with 80% infill density and grid fill pattern, while the conductive components are printed with carbon-filled TPU filament (Recreus Filaflex Conductive, Shore 92A, 1.4 M $\Omega \cdot m^{-1}$) using 100% infill density. Although both the materials are composed of TPU, the Recreus Filaflex Conductive is a composite that has carbon in its formulation, which enables conductive pathways in the printed capacitive plates and electrodes.

The capacitors and connections are subsequently positioned within the grooves and integrated into the metastructure through a soldering process, bringing the TPU above its melt transition temperature to fuse the two materials together. This fabrication allows for both the materials to seamlessly accommodate mechanical deformations with reduced mechanical mismatch, as they exhibit comparable mechanical properties.

B. Bistable Gripper

The unit cell incorporating the capacitive sensor is used as functional building block to design the bistable soft gripper. Two compliant mechanisms are attached to the left and right sides of the unit cell and convert linear motion into rotary motion. In this embodiment, the linear motion corresponds to the opening of the unit cell, which is converted into the rotation of two compliant pads that are connected to the bottom link of the mechanisms. Therefore, the gripper is composed of the unit cell, two compliant mechanisms, two pads, and additional structures that we named "holding and trigger extensions" and are directly attached to the two sides of the unit cell [Fig. 3(b)].

The natural stable configuration of the gripper is with the closed unit cell, whereas the ready-to-grasp configuration corresponds to the open unit cell, which is the second stable state or metastable. This is necessary as the force to close the gripper must be very small in order not to crush the object and the force to open it must be large to firmly hold the object. When the trigger extension comes into contact with an object, the reaction force exerted by the object causes the beams to snap into the closed configuration [Fig. 3(b)].

As a result, the gripping mechanisms also transition into a closed state, enabling the device to grasp and hold objects. As such, the bistable gripper is a passive mechanism that does not require actuation to perform a grasp. An external force or actuation is only required to reset the gripper in the ready-to-grasp configuration.

The bistable gripper is a monolithic piece fabricated via 3-D printing using TPU filament (NinjaTek Cheetah, Shore 95A) with 95% fill density and grid fill pattern, printed on a Prusa XL 5T printer. The conductive components are also 3-D-printed using a carbon-filled TPU filament (Recreus Filaflex Conductive, Shore 92A) with 100% fill density. In the multistable metastructure, the conductive components and electrical connections are positioned within the grooves and integrated into the bistable gripper by soldering. The gripper is printed in the closed configuration.

III. RESULTS AND DISCUSSION

We characterize the multistable metastructure under tensile load, using a uniaxial tensile testing machine (ZwickRoell Z010). The test is conducted by applying cycles of controlled displacement of 1 mm \cdot s⁻¹ to evaluate its nonlinear characteristic and to sense the mechanical state transitions sequence of the unit cells.

The bistable gripper is analyzed by grasping objects of different sizes and weight. In addition, we characterize the mechanical response of the unit cell in its open state under compression, to measure the amount of force required to trigger the closure mechanism. The gripper in the open configuration is fixed to the upper holder of the linear stage of the testing machine (ZwickRoell zwickiLine). To characterize the mechanical response, we move the gripper downward with controlled displacement (1 mm \cdot s⁻¹) until it touches the load cell of the testing machine (50 N max resolution). Regarding the grasping tests, we place the object to be grasped on the lower holder of the testing machines. The gripper approaches the object with a controlled displacement at 5 mm \cdot s⁻¹, and as

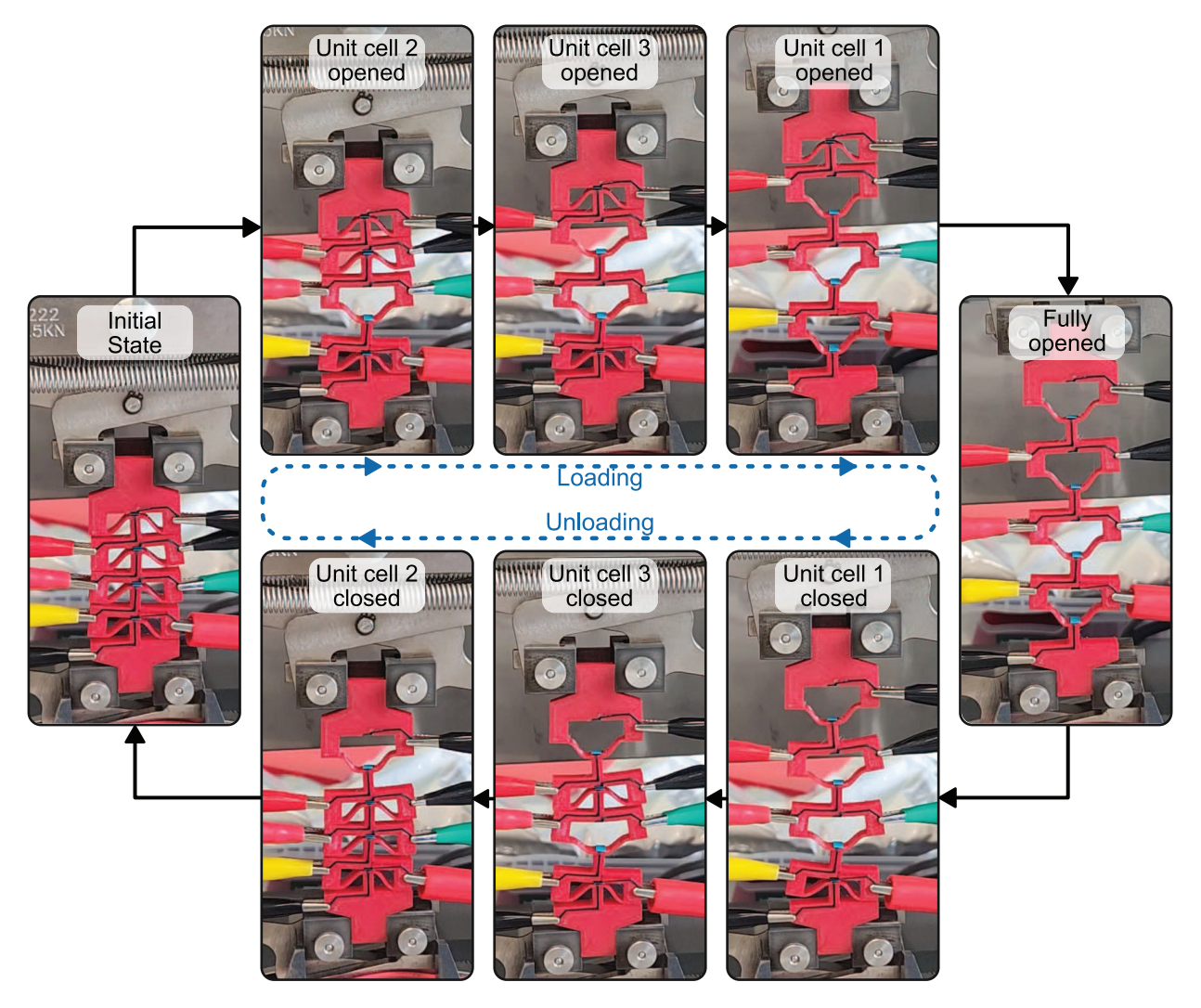


Fig. 4. Opening and closing cycle of the metastructure under cycling loading, illustrating the sequential transition of the unit cells from a fully closed state to a fully open state, and their subsequent return to the initial closed configuration.

soon as the trigger extension touches the object, the reaction force makes the unit cell snap and transition from the open state to the closed state, grasping the object.

The signals from the flexible capacitors in both the devices are acquired using a Texas Instruments FDC2214EVM board, which incorporates a chip FDC2214 with a 28-bit capacitanceto-digital converter [41]. Each pair of plates is connected to one of the board's four input channels. Rather than measuring capacitance directly, the FDC2214EVM drives an inductor–capacitor (*LC*) tank circuit whose resonant frequency shifts in response to the changes in the distance of the capacitive plates. Although the conductive TPU has a higher resistivity than typical metal electrodes, it remains sufficiently conductive at the operating frequency to establish the alternating electric field necessary for the resonant-frequency changing. The chip FDC2214 excites the circuit, detects the resulting resonant frequency shift, and maps this shift into a digital value. As the flexible conductive plates move closer or farther apart, their effective capacitance changes, causing the resonant frequency to shift accordingly. The board outputs a digital count proportional to the resonant frequency. Because of the chip's high sensitivity, this raw value includes a very

large static offset that makes small variations difficult to note. For this reason, an acquisition script performs a dynamic calibration that continuously tracks the highest and lowest sensor values. It then subtracts the current minimum value to remove the large static baseline signal. Finally, it scales this result to a 0–100 range, a process that makes the small variations clearly visible while automatically adapting to slow environmental drifts.

A. Multistable Metastructure

1) Mechanical Characterization: Fig. 4 shows the snapping sequence during the opening and closing of the unit cells under ten cycles of tensile loading for the multistable metastructure. Despite being fabricated with identical geometric parameters and 3-D printing settings, minor manufacturing imperfections cause slight variations in mechanical response, influencing which unit cell transitions between the open and closed states. Furthermore, during the loading cycles, all the unit cells undergo some degree of deformation prior to the transition of a particular unit cell from the open to the closed state.

When the metastructure is pulled, Unit Cell 2 (U2) is the first to switch mechanical state, followed by U3,

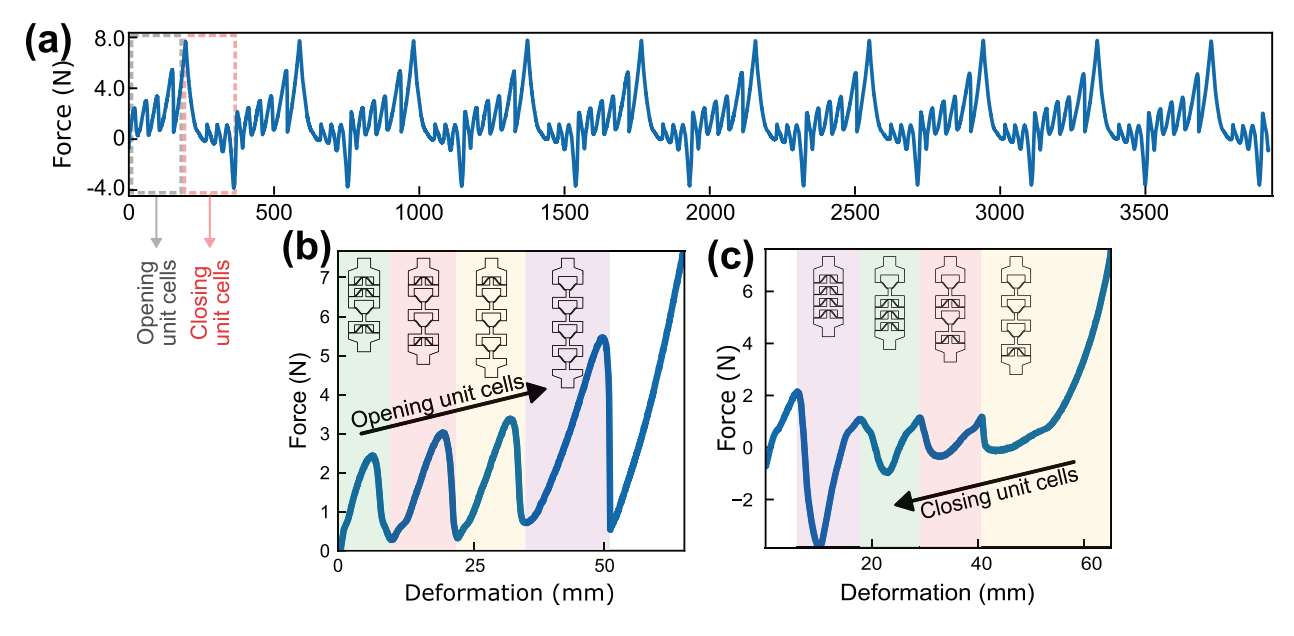


Fig. 5. Mechanical properties of the metastructure (a) Cyclic opening and closing of the metastructure, (b) force–deformation response illustrating the snapping sequence under tension, and (c) force–deformation response and snapping sequence during compression.

U1, and finally U4, corresponding to the fully opened configuration. Conversely, when the structure is released, the closing sequence begins with U1, followed by U3, U2, and U4. This sequence reveals an asymmetric behavior between the snapping events during opening and closing. In addition, this sequence is determined by manufacturing imperfections, although we demonstrated in a previous work that asymmetric sequences of multistable systems can be purposefully programmed by tuning the design of each snap-through structure. [13].

Fig. 5 shows the relationship between the mechanical deformation of the unit cells with their correspondent signal variation coming from each capacitive sensor. Fig. 5(a) illustrates ten tension–compression cycles and shows the consistent and repeatable nonlinear mechanical response of the structure. Fig. 5(b) depicts a single tensile cycle in which four distinct force peaks are observed, each corresponding to the snap-through transition of a unit cell. The colored background represents this transition for each unit cell. The structure's mechanical compliance is reflected in the low elastic forces exhibited during deformation, reaching up to 7 N.

Fig. 5(c) shows the unloading response of the snapping structure. The absolute force required to close each unit cell is lower than the force needed to open it. This difference arises from both the fabrication process, since the structure is manufactured in a fully closed configuration, and the nonlinear mechanics associated with the snap-through behavior. During opening, elastic energy is stored primarily in the curved beams and hinge regions until a critical point is reached, at which the structure snaps into the open state. Upon unloading, the release of stored elastic energy drives the structure back toward its original configuration, reducing the external force required for closure. However, because TPU is a viscoelastic material [42], part of the energy is dissipated, resulting in a significant hysteresis.

2) Electrical Properties: Fig. 6(a) shows the normalized sensor signals over ten cycles of opening and closing of the unit cells, shown in Fig. 5(a), demonstrating stable and repeatable behavior across all the four sensors. Min–Max normalization is applied to the signal conditioned through dynamic calibration during acquisition, defined as

$$y_i(n) = \frac{x_i(n) - x_{\min,i}(n)}{x_{\max,i}(n) - x_{\min,i}(n)}$$
 (2)

where $y_i(n)$ is the normalized signal from each sensor i, $x_i(n)$ is the signal acquired by the script at time step n, and $x_{\max,i}(n)$ and $x_{\min,i}(n)$ are the maximum and minimum observed values, respectively.

Fig. 6(b) and (c) illustrates the normalized signals acquired for each sensor during one opening and closing cycle of the unit cells, respectively. During cycling, all the unit cells experience some degree of deformation, which causes small separations in their capacitive plates, leading to changes in the acquired signals across all the sensors during each snapping event. However, only one unit cell transitions to a new mechanical state at each snapping event, causing its capacitive plates to shift from a fully closed to a fully open state (or vice versa), resulting in a greater variation in its capacitance. This is captured by the peaks in the Min-Max-normalized first time derivative of the acquired signal, shown in Fig. 6(d) and (e) for the opening and closing events, respectively. In each snapping event, the highest peak corresponds to the LC tank with the most significant frequency shift, indicating the unit cell that fully transitioned. In Fig. 6(e), the peaks are less distinct compared with the opening case; nevertheless, the snapping sequence remains identifiable.

In addition, mutual capacitance between adjacent electrodes contributes to signal interference, as the capacitors, electrical connections, and contacts are not electrically shielded. These effects are also influenced by parasitic capacitance, arising from the interactions between the electric fields of the

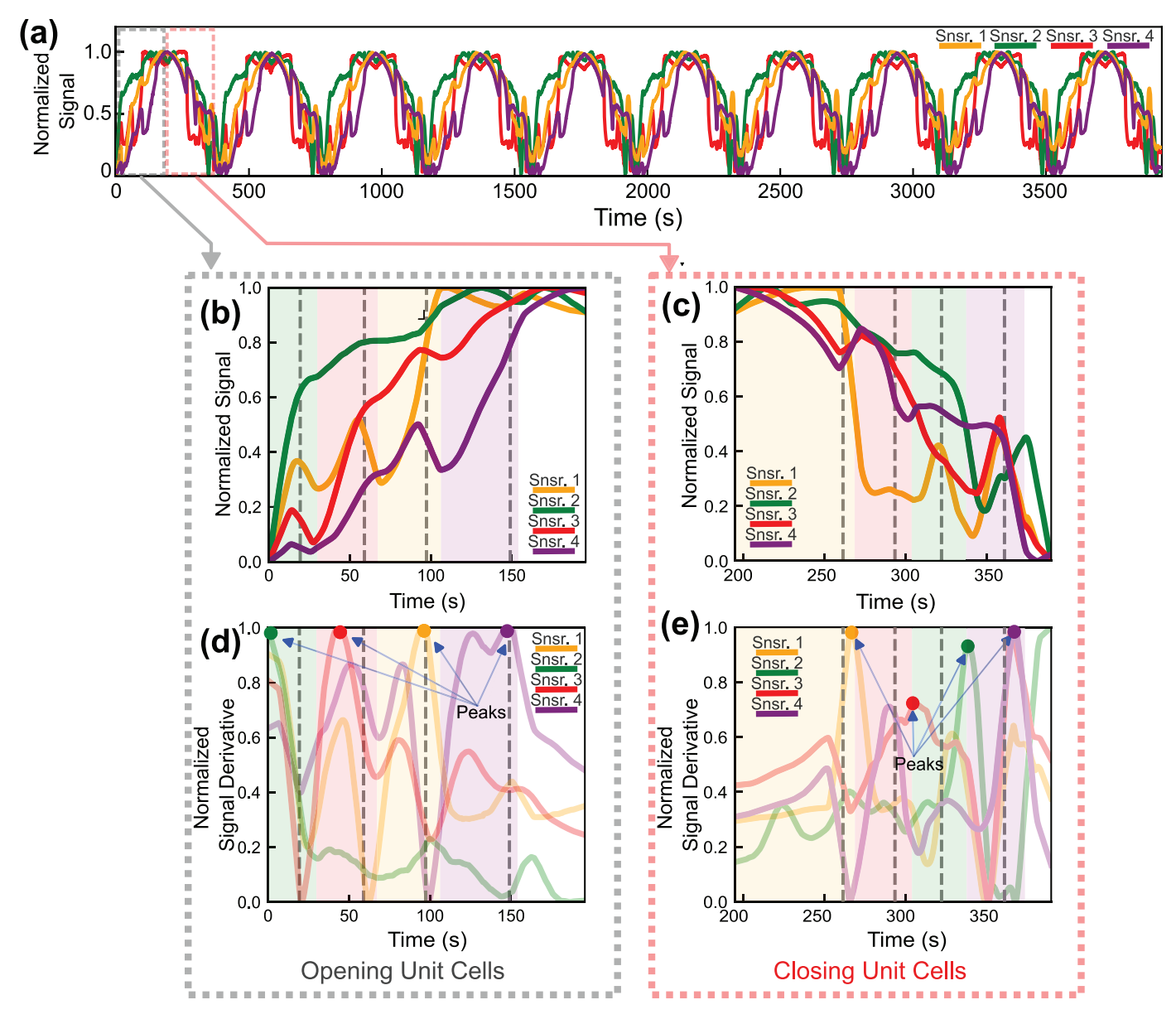


Fig. 6. Electrical properties of the metastructure (a) normalized signals obtained from the capacitive sensors during cyclic opening and closing of the unit cells, (b) normalized sensor signals corresponding to the opening of the unit cells, (c) normalized sensor signals corresponding to the closing of the unit cells, (d) normalized first derivative of sensor signals during opening of the unit cells, and (e) normalized first derivative of sensor signals during closing of the unit cells.

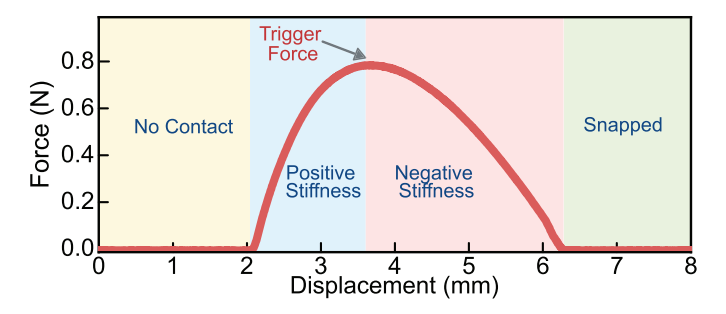


Fig. 7. Mechanical characterization of the gripper unit cell under compression.

capacitors and nearby electrical paths. This parasitic coupling alters the effective capacitance of each sensor, introducing additional variations across all the sensing elements. Nevertheless, the signal variation from the sensor attached to the snapping unit cell remains more pronounced due to the rapid and large displacement between its capacitive plates.

This analysis enables the identification of the snapping sequence during both opening and closing of the structure. Based on the geometry of the capacitive plates, the estimated capacitance for each sensor is approximately 0.025 pF in the open state and 0.750 pF in the closed state.

3) Proprioceptive Properties: The state transitions of the mechanical metastructure are captured through the variation in the sensor signal, which arises from the changes in the distance between the conductive plates during deformation. By combining the time required for each unit cell to snap with the largest variation of the signal within that interval, it is possible to identify the snapping sequence of the unit cells

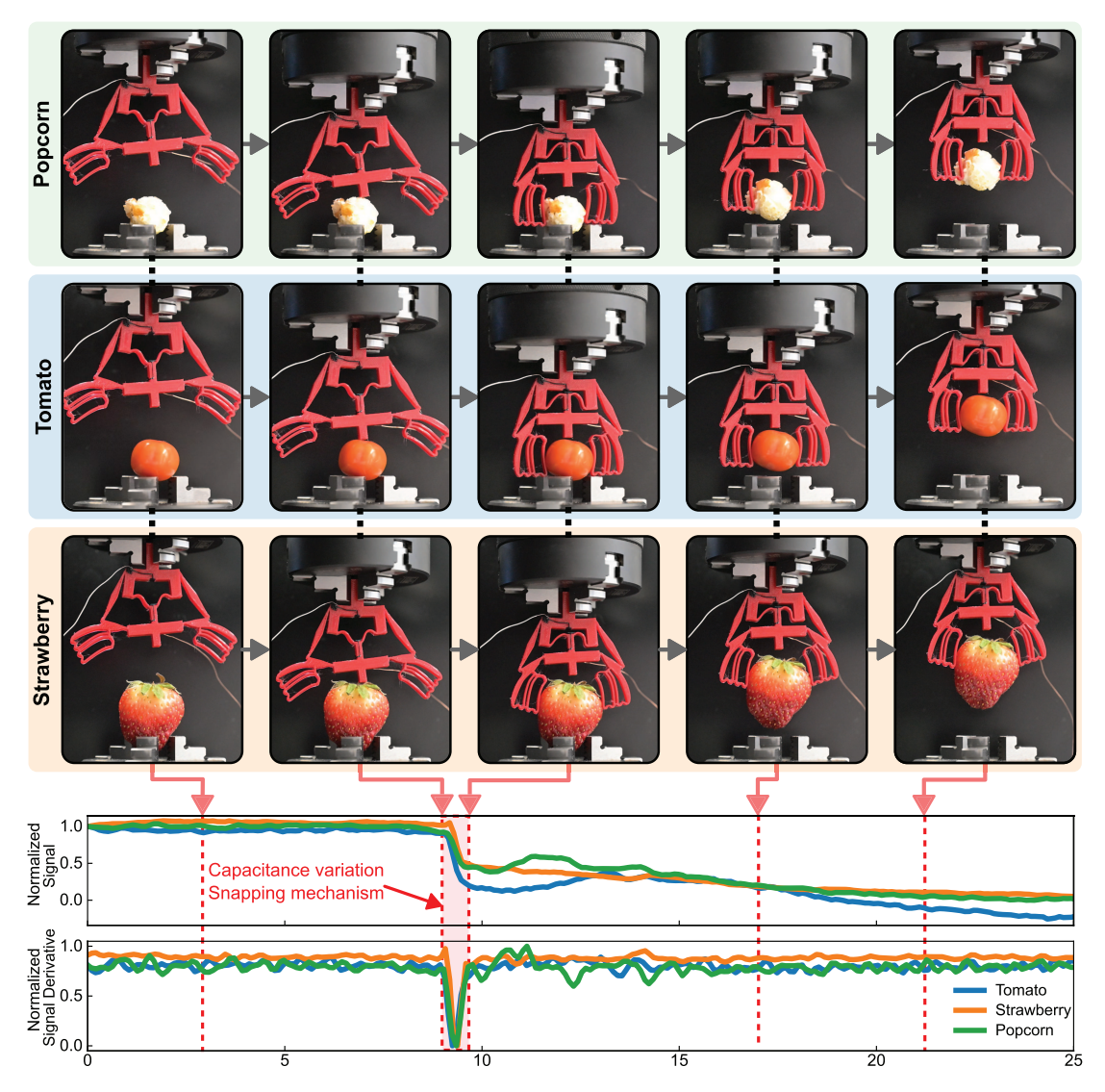


Fig. 8. Demonstration of a bistable soft gripper that uses the metastructure-based unit cell with integrated capacitive sensing. The gripper securely handles a popcorn, a tomato, and a strawberry, with a weight ranging from 0.5 to 16 g. The normalized capacitive signal and its first derivative clearly identify grasping events, providing proprioceptive feedback critical for operation without visual monitoring.

and, consequently, determine the global mechanical state of the structure at any given time.

This integration of sensors gives the metastructure proprioceptive capabilities, namely, the ability to sense its own state transitions. Indeed, in real-world applications, the snapping sequence may deviate from that observed under quasi-static conditions. Localized external forces, dynamic loading, and fatigue effects introduce uncertainties that affect the mechanical response and shift the snapping thresholds. With integrated proprioceptive monitoring, the metastructure can track its actual sequence of state transitions in real-time, providing resilience to environmental and operational changes.

B. Bistable Soft Gripper

To demonstrate the integration of capacitive sensors not only in mechanical metamaterials but also in functional soft machines, the proposed unit cell is used as an activation mechanism for a bistable soft gripper that can grasp and hold objects. The snapping of the unit cell drives the closing motion of the gripping mechanisms, which bend around and secure the object. The gripper is subsequently moved upward, lifting the grasped object.

The mechanical response of the gripper's unit cell is depicted in Fig. 7. At the beginning of the controlled displacement, the gripper moves toward the load cell, which does not measure any force as there is no contact yet (yellow area in the figure). As soon as the gripper touches the load cell via its trigger extension, the force starts to ramp up, showing a normal positive stiffness trend (blue area). At a critical force of 0.8 N, the unit cell enters a negative stiffness region (red area) where the force decreases as the displacement increases. As soon as the force reaches the zero point, the unit cell snaps closed, losing contact with the load cell (green area). Therefore, the gripper closing mechanism is triggered as soon as the reaction force exerted by the object passes the force peak of 0.8 N.

Fig. 8 and the supplemental video show examples of very delicate and fragile items being manipulated by the gripper: a

popcorn (0.5 g), a cherry tomato (12 g), and a fresh strawberry (16 g). Those objects can largely sustain the trigger force of 0.8 N without being crushed and, despite differences in weight and sizes, all the objects are firmly grasped and safely lifted, demonstrating the versatility and potential of bistable unit cells for applications in soft robotics.

Fig. 8 also presents the normalized signal obtained from the *LC* tank associated with the flexible capacitor integrated into the unit cell. Like the multistable structure, the dynamically calibrated signal is Min–Max-normalized to scale it within the range 0–1, facilitating the comparison between the grasping of the three different items. Prior to object contact, the normalized signal exhibits minimal variation. When the trigger extension touches the object and snaps, the signal drops significantly, indicating a mechanical transition from a fully open to a fully closed state. This results in a change in the sensor's capacitance and, consequently, a shift in the resonant frequency. The differentiation of this signal with respect to time, followed by Min–Max normalization, reveals a distinct peak precisely during the snapping transition, as shown in Fig. 8.

Following the grasping event and subsequent vertical movement, the normalized signal continues to decrease in all the three cases. This gradual reduction may be attributed to various factors, including parasitic capacitance or noise originating from the motion platform itself. The gripper's mechanical stability may also play a significant role in the signal variation after grasping the items, as the capacitive plates might become misaligned, reducing their overlap. In addition, the proximity of the grasped objects to the capacitive plates may influence the resonant frequency of the sensor's circuit. However, the derivative of the normalized signal remains stable after the peak, indicating that no further snapping events occur.

Through the analysis of the signal variation, it becomes possible to infer the snapping transitions in real-time, effectively providing proprioceptive capabilities. This information reveals whether the structure has been activated or not. Such proprioceptive sensing is highly valuable for the development and control of soft robotic systems, particularly in scenarios where visual feedback is unavailable and it is not possible to directly observe whether the gripper has snapped closed or not. Soft capacitive sensors offer a reliable alternative to other sensing technologies, such as piezoresistive sensors or contact switches. Compared with piezoresistive sensors, our sensors have a quicker response time and do not experience significant mechanical strain, making them more durable and repeatable. Moreover, compared with contact switches, our sensors do not require direct contact between conductive elements, which could introduce forces that alter the nonlinear response of the soft machines while also limiting life cycles due to wear. Conversely, the major disadvantages of capacitive technology lay in the extreme sensitivity to environmental factors and the continuous power consumption required for operation.

IV. CONCLUSION

This work demonstrates how integrating soft capacitive sensors into multistable soft machines, such as multistable metastructures and bistable grippers, enables proprioceptive capabilities, which are key to develop autonomous soft robots. Capacitive sensors are used as contactless switches to detect the mechanical state transitions of the multistable structure, enabling their use despite their simplicity and low sensitivity. By coupling a metastructure composed of four bistable unit cells with soft printed capacitive plates, we identified distinct snapping events in both tensile loading and unloading modes, tracking state transitions through capacitance changes ranging from 0.75 to 0.025 pF. Under repeated cycles, the metastructure consistently snapped at forces around 7 N, confirming stable and repeatable performance. Furthermore, the same sensing approach was integrated into a soft gripper, enabling secure grasping of several delicate objects, like a fresh strawberry, a tomato, and a popcorn spanning 0.5–16 g. Both the metastructure and gripper are entirely fabricated from TPU-based filaments using commercial 3-D printing, ensuring mechanical compliance while allowing design freedom. This fully 3D-printed approach uses thermoplastic elastomers for both structural and conductive components, enabling a seamless fabrication process that ensures mechanical compatibility.

Future work will focus on refining sensor designs to reduce parasitic and mutual capacitance and minimize environmental sensitivity, along with integrating smaller, higher resolution electronics. This is a key step toward developing integrated, closed-loop soft robotic systems. As these technologies advance, soft robotics and electronics will become more tightly integrated, paving the way to fully compliant, autonomous machines that harness multistability for more sophisticated and adaptive tasks, combining soft electronic circuitry with physical control elements enabled by the peculiar mechanical and electrical properties of soft matter.

REFERENCES

- C. Laschi, B. Mazzolai, and M. Cianchetti, "Soft robotics: Technologies and systems pushing the boundaries of robot abilities," *Sci. Robot.*, vol. 1, no. 1, p. 3690, Dec. 2016.
- [2] F. Hartmann, M. Baumgartner, and M. Kaltenbrunner, "Becoming sustainable, the new frontier in soft robotics," *Adv. Mater.*, vol. 33, no. 19, May 2021, Art. no. 2004413.
- [3] M. Cianchetti, C. Laschi, A. Menciassi, and P. Dario, "Biomedical applications of soft robotics," *Nature Rev. Mater.*, vol. 3, no. 6, pp. 143–153, May 2018.
- [4] S. Aracri et al., "Soft robots for ocean exploration and offshore operations: A perspective," Soft Robot., vol. 8, no. 6, pp. 625–639, Dec. 2021.
- [5] C. Della Santina, M. G. Catalano, and A. Bicchi, Soft Robots. Berlin, Germany: Springer, 2021, pp. 1–15.
- [6] N. S. Usevitch, Z. M. Hammond, M. Schwager, A. M. Okamura, E. W. Hawkes, and S. Follmer, "An untethered isoperimetric soft robot," *Sci. Robot.*, vol. 5, no. 40, p. 0492, Mar. 2020.
- [7] E. Milana, B. Gorissen, E. De Borre, F. Ceyssens, D. Reynaerts, and M. De Volder, "Out-of-plane soft lithography for soft pneumatic microactuator arrays," *Soft Robot.*, vol. 10, no. 1, pp. 197–204, Feb. 2023
- [8] C. Majidi, "Soft-matter engineering for soft robotics," Adv. Mater. Technol., vol. 4, no. 2, 2018, Art. no. 1800477.
- [9] Y. Chi, Y. Li, Y. Zhao, Y. Hong, Y. Tang, and J. Yin, "Bistable and multistable actuators for soft robots: Structures, materials, and functionalities," *Adv. Mater.*, vol. 34, no. 19, May 2022, Art. no. 2110384.
- [10] J. T. B. Overvelde, T. Kloek, J. J. A. D'haen, and K. Bertoldi, "Amplifying the response of soft actuators by harnessing snapthrough instabilities," *Proc. Nat. Acad. Sci. USA*, vol. 112, no. 35, pp. 10863–10868, Sep. 2015.
- [11] F. Pan et al., "Miniature deep-sea morphable robot with multimodal locomotion," Sci. Robot., vol. 10, no. 100, p. 7821, Mar. 2025. [Online]. Available: https://www.science.org/doi/abs/10.1126/scirobotics.adp7821

- [12] B. Gorissen, D. Melancon, N. Vasios, M. Torbati, and K. Bertoldi, "Inflatable soft jumper inspired by shell snapping," *Sci. Robot.*, vol. 5, no. 42, p. 1967, May 2020.
- [13] B. Van Raemdonck, E. Milana, M. De Volder, D. Reynaerts, and B. Gorissen, "Nonlinear inflatable actuators for distributed control in soft robots," *Adv. Mater.*, vol. 35, no. 35, Sep. 2023, Art. no. 2301487.
- [14] E. Milana, B. Van Raemdonck, A. S. Casla, M. De Volder, D. Reynaerts, and B. Gorissen, "Morphological control of cilia-inspired asymmetric movements using nonlinear soft inflatable actuators," *Frontiers Robot. AI*, vol. 8, Jan. 2022, Art. no. 788067.
- [15] L. C. van Laake, J. de Vries, S. Malek Kani, and J. T. B. Overvelde, "A fluidic relaxation oscillator for reprogrammable sequential actuation in soft robots," *Matter*, vol. 5, no. 9, pp. 2898–2917, Sep. 2022.
- [16] P. Rothemund et al., "A soft, bistable valve for autonomous control of soft actuators," *Sci. Robot.*, vol. 3, no. 16, p. 7986, Mar. 2018. [Online]. Available: https://www.science.org/doi/full/10.1126/scirobotics.aar7986
- [17] C. Della Santina, C. Duriez, and D. Rus, "Model-based control of soft robots: A survey of the state of the art and open challenges," *IEEE Control Syst.*, vol. 43, no. 3, pp. 30–65, Jun. 2023.
- [18] E. Milana, F. Stella, B. Gorissen, D. Reynaerts, and C. D. Santina, "Model-based control can improve the performance of artificial cilia," in *Proc. IEEE 4th Int. Conf. Soft Robot. (RoboSoft)*, Apr. 2021, pp. 527–530.
- [19] C. Hegde, J. Su, J. M. R. Tan, K. He, X. Chen, and S. Magdassi, "Sensing in soft robotics," ACS nano, vol. 17, no. 16, pp. 15277–15307, 2023
- [20] J.-H. Lee, K. Cho, and J.-K. Kim, "Age of flexible electronics: Emerging trends in soft multifunctional sensors," *Adv. Mater.*, vol. 36, no. 16, Apr. 2024, Art. no. 2310505, doi: 10.1002/adma.202310505.
- [21] H. de Souza Oliveira et al., "Mechanical metamaterial sensors: From design to applications," *J. Phys. D: Appl. Phys.*, vol. 58, no. 13, Feb. 2025, Art. no. 133002, doi: 10.1088/1361-6463/adade5.
- [22] N. Saeedzadeh Khaanghah et al., "Application of stone-derived substrates in thin-film temperature sensing," *IEEE Sensors J.*, vol. 24, no. 24, pp. 40179–40187, Dec. 2024.
- [23] L. Migliorini, T. Santaniello, A. Falqui, and P. Milani, "Super-stretchable resistive strain sensor based on ecoflex-gold nanocomposites," ACS Appl. Nano Mater., vol. 6, no. 10, pp. 8999–9007, May 2023.
- [24] J. D. Hubbard et al., "Fully 3D-printed soft robots with integrated fluidic circuitry," Sci. Adv., vol. 7, no. 29, p. 5257, Jul. 2021. [Online]. Available: http://www.science.org/doi/full/10.1126/sciadv.abe5257
- [25] Y. Zhai et al., "Desktop fabrication of monolithic soft robotic devices with embedded fluidic control circuits," *Sci. Robot.*, vol. 8, no. 79, p. 3792, Jun. 2023. [Online]. Available: https://www.science.org/doi/pdf/ 10.1126/scirobotics.adg3792
- [26] S. Conrad et al., "3D-printed digital pneumatic logic for the control of soft robotic actuators," *Sci. Robot.*, vol. 9, no. 86, Jan. 2024, Art. no. eadh4060.
- [27] L. Scimeca, J. Hughes, P. Maiolino, and F. Iida, "Model-free soft-structure reconstruction for proprioception using tactile arrays," *IEEE Robot. Autom. Lett.*, vol. 4, no. 3, pp. 2479–2484, Jul. 2019.

- [28] P. Maiolino, F. Galantini, F. Mastrogiovanni, G. Gallone, G. Cannata, and F. Carpi, "Soft dielectrics for capacitive sensing in robot skins: Performance of different elastomer types," Sens. Actuators A, Phys., vol. 226, pp. 37–47, May 2015.
- [29] Z. Xie, F. Yuan, Z. Liu, Z. Sun, E. M. Knubben, and L. Wen, "A proprioceptive soft tentacle gripper based on crosswise stretchable sensors," IEEE/ASME Trans. Mechatronics, vol. 25, no. 4, pp. 1841–1850, Aug. 2020.
- [30] N. Hanson, I. A. Mensah, S. F. Roberts, J. Healey, C. Wu, and K. L. Dorsey, "Controlling the fold: Proprioceptive feedback in a soft origami robot," *Frontiers Robot. AI*, vol. 11, May 2024, Art. no. 1396082
- [31] A. López-Díaz et al., "Proprioception and control of a soft pneumatic actuator made of a self-healable hydrogel," *Soft Robot.*, vol. 11, no. 5, pp. 889–901, Oct. 2024.
- [32] K.-Y. Lin, A. Gamboa-Gonzalez, and M. Wehner, "Soft robotic sensing, proprioception via cable and microfluidic transmission," *Electronics*, vol. 10, no. 24, p. 3166, Dec. 2021.
- [33] I. M. Van Meerbeek, C. M. De Sa, and R. F. Shepherd, "Soft optoelectronic sensory foams with proprioception," *Sci. Robot.*, vol. 3, no. 24, p. 2489, Nov. 2018.
- [34] E. De Smet, L. Migliorini, E. Milana, P. Milani, and B. Gorissen, "Electropneumatic oscillators using nonlinear inflatables," Adv. Intell. Syst., vol. 7, no. 6, Jun. 2025, Art. no. 2400695.
- [35] J. Qu et al., "Advanced flexible sensing technologies for soft robots," Adv. Funct. Mater., vol. 34, no. 29, Jul. 2024, Art. no. 2401311.
- [36] S. Mousavi, D. Howard, F. Zhang, J. Leng, and C. H. Wang, "Direct 3D printing of highly anisotropic, flexible, constriction-resistive sensors for multidirectional proprioception in soft robots," ACS Appl. Mater. Interface, vol. 12, no. 13, pp. 15631–15643, Apr. 2020.
- [37] T. G. Thuruthel, S. Haider Abidi, M. Cianchetti, C. Laschi, and E. Falotico, "A bistable soft gripper with mechanically embedded sensing and actuation for fast grasping," in *Proc. 29th IEEE Int. Conf. Robot Human Interact. Commun. (RO-MAN)*, Aug. 2020, pp. 1049–1054.
- [38] D. Restrepo, N. D. Mankame, and P. D. Zavattieri, "Phase transforming cellular materials," *Extreme Mech. Lett.*, vol. 4, pp. 52–60, Sep. 2015. [Online]. Available: https://www.sciencedirect.com/science/article/pii/S2352431615000929
- [39] S. Shan et al., "Multistable architected materials for trapping elastic strain energy," Adv. Mater., vol. 27, no. 29, pp. 4296–4301, Aug. 2015. [Online]. Available: https://onlinelibrary.wiley.com/doi/pdf/10.1002/adma.201501708
- [40] H. Yang and L. Ma, "Multi-stable mechanical metamaterials by elastic buckling instability," *J. Mater. Sci.*, vol. 54, no. 4, pp. 3509–3526, Feb. 2019.
- [41] J. Gong, O. Seow, C. Honnet, J. Forman, and S. Mueller, "MetaSense: Integrating sensing capabilities into mechanical metamaterial," in *Proc. 34th Annu. ACM Symp. User Interface Softw. Technol.*, 2021, pp. 1063–1073, doi: 10.1145/3472749.3474806.
- [42] C. Emminger, A. Kapshammer, J. Birtha, U. Cakmak, J. Fischer, and Z. Major, "Improving damping performance of thermoplastic composite materials through SMC-TPU hybridization," *J. Appl. Polym. Sci.*, vol. 142, no. 22, Jun. 2025, Art. no. e56938, doi: 10.1002/app.56938.